Superlattices and Microstructures 115 (2018) 10–18

Contents lists available at ScienceDirect

Superlattices and Microstructures

journal homepage: www.elsevier.com/locate/superlattices

First principles study of optical properties of molybdenum disulfide: From bulk to monolayer

Nguyen N. Hieu [a], Victor V. Ilyasov [b], Tuan V. Vu [c], Nikolai A. Poklonski [d], Huynh V. Phuc [e], Le T.T. Phuong [f], Bui D. Hoi [f], Chuong V. Nguyen [g, *]

[a] Institute of Research and Development, Duy Tan University, Da Nang, Viet Nam
[b] Department of Physics, Don State Technical University, Rostov–on–Don, Russia
[c] Center of Experiment and Practice, University of Food Industry, Ho Chi Minh, Viet Nam
[d] Department of Physics, Belarusian State University, Minsk, Belarus
[e] Division of Theoretical Physics, Dong Thap University, Dong Thap, Viet Nam
[f] Department of Physics, University of Education, Hue University, Hue, Viet Nam
[g] Department of Materials Science and Engineering, Le Quy Don Technical University, Ha Noi, Viet Nam

ARTICLE INFO

Article history:
Received 19 December 2017
Received in revised form 12 January 2018
Accepted 12 January 2018
Available online 19 January 2018

Keywords:
Ab-initio
MoS_2
Optical properties

ABSTRACT

In this paper, we theoretically study the optical properties of both bulk and monolayer MoS_2 using first-principles calculations. The optical characters such as: dielectric function, optical reflectivity, and electron energy-loss spectrum of MoS_2 are observed in the energy region from 0 to 15 eV. At equilibrium state the dielectric constant in the parallel $E_{\|x}$ and perpendicular $E_{\|z}$ directions are of 15.01 and 8.92 for bulk while they are 4.95 and 2.92 for monolayer MoS_2, respectively. In the case of bulk MoS_2, the obtained computational results for both real and imaginary parts of the dielectric constant are in good agreement with the previous experimental data. In the energy range from 0 to 6 eV, the dielectric functions have highly anisotropic, whereas they become isotropic when the energy is larger than 7 eV. For the adsorption spectra and optical reflectivity, both the collective plasmon resonance and $(\pi + \sigma)$ electron plasmon peaks are observed, in which the transition in $E_{\|x}$ direction is accordant with the experiment data more than the transition in $E_{\|z}$ direction is. The refractive index, extinction index, and electron energy-loss spectrum are also investigated. The observed prominent peak at 23.1 eV in the energy-loss spectra is in good agreement with experiment value. Our results may provide a useful potential application for the MoS_2 structures in electronic and optoelectronic devices.

© 2018 Elsevier Ltd. All rights reserved.

1. Introduction

Graphene [1], a two-dimensional (2D) materials in the single atomic layer, has attracted great interest for applications in nanoelectronic technology due to their unique transport properties [2–6]. However, the clean graphene does not have a band gap in its electronic structure, which is deemed as a considerable drawback for many applications, in optics and transistor technology. This limitation of graphene leads researchers to investigate alternate materials that are similar to graphene and distinct in their electronic properties. In recent year, transition metal dichalcogenides (TMDs) have have become of great

* Corresponding author.
E-mail address: chuongnguyen11@gmail.com (C.V. Nguyen).

https://doi.org/10.1016/j.spmi.2018.01.012
0749-6036/© 2018 Elsevier Ltd. All rights reserved.

interest due to their novel mechanical, transport, and optical properties [7–14]. Among them, molybdenum disulfide (MoS_2) is currently one of most interesting materials for applications in nano-electronic and optoelectronic devices due to its unique electronic, mechanical, transport, and optical properties [15–20].

The MoS_2 bulk is a semiconductor with an indirect electronic band gap of the 1.24 eV opening between the highest energy state of the valence bands located at the Γ point and the lowest energy state of the conduction bands located between the Γ and *K* points. Whereas, the MoS_2 monolayer is the semiconductor with a direct band gap of the 1.80 eV [7] opening between the highest/lowest energy state of the valence/conduction bands located at the *K* point. Moreover, MoS_2 monolayer has been successfully synthesized by various experimental techniques, such as chemical vapor deposition [21], micromechanical cleavage [22], or liquid exfoliation [23]. The indirect–direct band gap transition makes MoS_2 nanomaterial being a promising potential material for application in optoelectronics [24]. Recently, the structure of both bulk and monolayer MoS_2 has been studied by density functional theory (DFT) [25]. Effect of uniaxial strain and external electric field on electronic properties of both bulk and monolayer MoS_2 has also been considered by different methods [16,26–29]. Besides, optical properties of MoS_2 have attracted many scientists [30–33]. Using DFT calculations, they have shown that the blue-shift phenomenon was observed in O–doped MoS_2 systems [11]. The static dielectric constant of the monolayer MoS_2 with neutral S and Mo vacancies is respectively 1.50 and 2.45, and the S vacancy does not effect on the static dielectric constant of the monolayer MoS_2 [34]. Recently, we theoretically studied the magneto-optical absorption coefficient of MoS_2 on polar substrates in the presence of an external magnetic field [35].

In the present work, we study the optical properties of the MoS_2 using DFT calculations. We calculate the optical characters of both bulk and monolayer MoS_2. Effect of direction of an external electric field on the dielectric constant and other optical characters is also considered and discussed.

2. Theoretical model and method

In this paper, DFT calculations of electronic and optical properties of bulk and monolayer MoS_2 were performed employing the APW + lo method [36]. The full potential which not depends on any predefined form, such as muffin-tin one was adopted in the present calculations. The muffin-tin (MT) sphere radii of atoms constituting the MoS_2 system were supposed to be equal to 2.27 a.u. for Mo and 1.95 a.u. for S in bulk MoS_2 and 2.44 a.u. for Mo and 2.1 a.u. for S in monolayer MoS_2.

Inside the atomic spheres for wave function expansion, the maximum value of orbital quantum number *l* is confined to $l_{max} = 10$. In the interstitial region, the wave functions were extended regarding plane waves with the cut-off value of $RK_{max} = 7$. Besides, magnitude of largest vector in Fourier expansion of the charge density was set to $G_{max} = 12$ (a.u)$^{-1}$. All these values have been chosen in a way to ensure the convergence of the results. These above-mentioned parameters are used further for the calculations of the electronic structure and optical properties of both bulk and monolayer MoS_2.

For calculations of the exchange-correlation potential, generalized gradient approximation (GGA) by Perdew-Burke-Ernzerhof (PBE) [37,38] potential was used. Further, the tetrahedron method by Blochl et al. [39] was employed for integration through the Brillouin zone (BZ). The BZ sampling was made using 1000 *k*-points within the full zone. The iteration process was verified accounting changes in the integral charge difference $q = \int |\rho_n(r) - \rho_{n-1}(r)| dr$, where $\rho_{n-1}(r)$ and $\rho_n(r)$ are input previous iteration and output current iteration charge density, respectively, and the calculations were intercepted when reaching the value $q \leq 10^{-4}$.

3. Results and discussion

Atomic structure of MoS_2 is shown in Fig. 1. It can be seen that MoS_2 crystal has the hexagonal structure, which consists of S–Mo–S layers. In each layer, the Mo atoms are arranged in the hexagonal lattice and positioned in trigonal prismatic coordination with the two S layers. After relaxation, the lattice constants of bulk and monolayer MoS_2 are 3.176 Å and 3.180 Å, respectively. This result is in good agreement with the previous theoretical calculations [25,31] and the experimental measurements [7,40]. Moreover, our obtained Mo–S bond length in both MoS_2 bulk and monolayer is 1.41 Å, which is consistent with the experimental value [7]. In Fig. 2 we display the electronic band structures of both MoS_2 bulk and monolayer. We found that MoS_2 bulk is a semiconductor with an indirect band gap, opening between the highest occupied energy state of the valence band located at the Γ point and the lowest unoccupied energy state of the conduction band located at the *K* point. When MoS_2 bulk is transformed to a monolayer, it becomes a semiconductor with a direct band gap, opening between the highest occupied state of the valence band and the lowest unoccupied state of the conduction band located at the *K* point. Our calculated band gaps for the bulk and monolayer MoS_2 are respectively 1.23 eV and 1.70 eV which are in good agreement with the available data [7,41].

We next focus on the optical properties of MoS_2 bulk and monolayer in the energy range from 0 to 15 eV. Real and imaginary parts of dielectric function for bulk and monolayer MoS_2 are calculated by considering interband transition for both directions of electric field: (i) parallel $E_{\|x}$ and (ii) perpendicular $E_{\|z}$. The $\varepsilon_2(\omega)$ constituents are worth to be known for depiction of the linear optical susceptibility of the crystal and they are denoted as follows [42]:

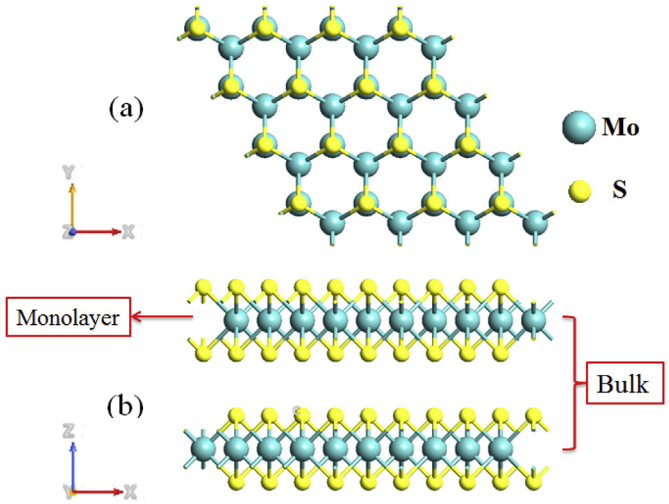

Fig. 1. The top view (a) and side view (b) of the atomic structure of the MoS_2. The green and yellow balls stand for the Mo and S atoms, respectively. (For interpretation of the references to colour in this figure legend, the reader is referred to the Web version of this article.)

$$\varepsilon_2^{ij}(\omega) = \frac{4\pi^2 e^2}{Vm^2\varpi^2}\sum_{nn'\sigma}\langle kn\sigma\left|p_i\right|kn'\sigma\rangle\langle kn'\sigma\left|p_j\right|kn\sigma\rangle \times f_{kn}(1-f_{kn'})\delta(E_{kn'}-E_{kn}-\hbar\omega), \tag{1}$$

where e and m stand respectively for the charge and mass of electron, ω is the angular frequency of electromagnetic irradiation, V is a unit-cell volume, p is the momentum operator, $|knp\rangle$ is the wave function of a crystal with crystal wave vector $\overrightarrow{k}$, σ is spin which corresponds to the energy eigenvalue E_{kn}, and f_{kn} is the Fermi distribution function bringing a certain count to transitions from occupied states to unoccupied states.

The real part $\varepsilon_1(\omega)$ and imaginary $\varepsilon_2(\omega)$ parts of dielectric function $\varepsilon(\omega) = \varepsilon_1(\omega) + i\varepsilon_2(\omega)$ for bulk and monolayer MoS_2 are obtained by the Kramers-Kronig transformation from its corresponding imaginary part as following [43]:

$$\varepsilon_1(\omega) = 1 + \frac{2}{\pi}P\int_0^\infty \frac{\omega'\varepsilon_2(\omega')}{\omega'^2-\omega^2}d\omega', \tag{2}$$

where P stands for the principal value of the integral.

In Fig. 3 we presented the real and imaginary parts of the dielectric function of both bulk and monolayer MoS_2. We can see that the dielectric function for MoS_2 bulk is completely different from the dielectric function of MoS_2 monolayer and the values of dielectric constants are different in the out-plane and in-plane directions of the electric field. At equilibrium state the dielectric constant in the parallel $E_{\|x}$ and perpendicular $E_{\|z}$ directions is 15.01 and 8.92 for bulk MoS_2, respectively. The dielectric constant is 4.95 and 2.92 for monolayer MoS_2 in $E_{\|x}$ and $E_{\|z}$, respectively [see Fig. 3(a)]. Fig. 3 shows that, in the energy range from 0 to 6 eV, the dielectric functions have highly anisotropic, while they become isotropic when the energy is larger than 7 eV.

In Fig. 3(a,c), we also showed the dielectric functions of bulk MoS_2 in comparison with the experimental results. Our calculations for both real ε_1 and imaginary ε_2 parts of the dielectric constant of bulk MoS_2 are in good agreement with the previous experimental measurements [44]. The imaginary part of the dielectric function for bulk MoS_2 has three structure peaks A, B, and C (counts both $E_{\|x}$ and $E_{\|z}$) at the energy of 2.8 eV, 4.4 eV, and 5.5 eV, respectively, as shown in Fig. 3(c). While, the imaginary part of dielectric functions for MoS_2 monolayer shows four structure peaks A, B, C, and D at the energy of 2.9 eV, 3.7 eV, 4.4 eV, and 5.2 eV, respectively. It is shown that the additional structure peak B at the energy of 3.7 eV is appeared for monolayer MoS_2 in comparison with bulk MoS_2, as shown in Fig. 3(d).

Fig. 4 shows the adsorption coefficient $\alpha(\omega)$ and optical reflectivity $R(\omega)$ of bulk and monolayer MoS_2 in both $E_{\|x}$ and $E_{\|z}$ directions. It is known that the optical absorption spectrum is vital in investigating the optical properties of MoS_2. The absorption coefficient $\alpha(\omega)$ and reflectance can be calculated as follows

$$\alpha^{ij}(\omega) = \frac{2\omega k^{ij}(\omega)}{c}, \tag{3}$$

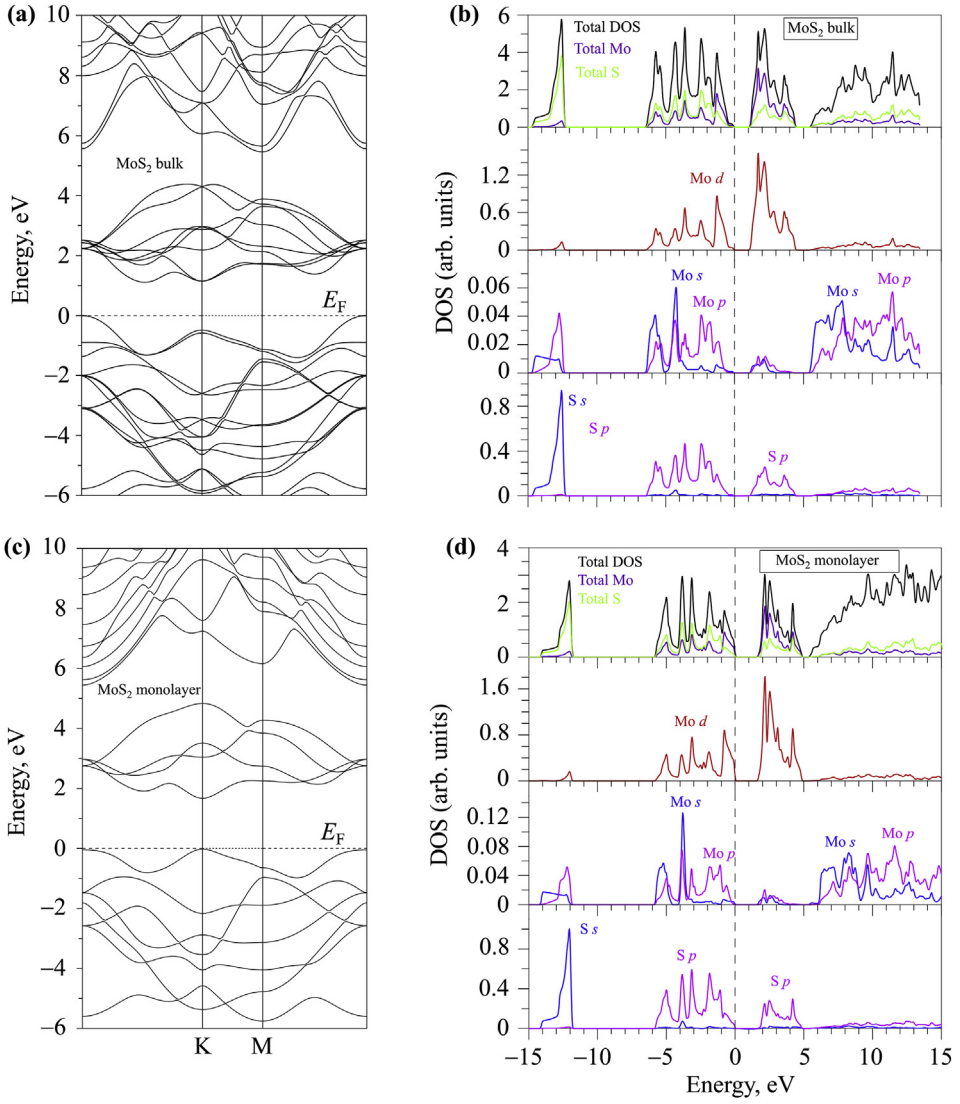

Fig. 2. Electronic band structure and density of states of the bulk MoS_2 (a) and (b) and monolayer MoS_2 (c) and (d), respectively. The Fermi energy level is set to 0 eV.

$$R^{ij}(\omega) = \frac{\left(n^{ij}-1\right)^2 + k^{ij^2}}{\left(n^{ij}-1\right)^2 - k^{ij^2}} = \left|\frac{\sqrt{\varepsilon_1^{ij} + i\varepsilon_2^{ij}} - 1}{\sqrt{\varepsilon_1^{ij} + i\varepsilon_2^{ij}} + 1}\right|^2. \tag{4}$$

As shown in Fig. 4(a), for bulk MoS_2 in $E_{\|x}$ direction, the minimum of adsorption spectra is observed about 8.8 eV associated with the collective plasmons resonance, whereas the first and the highest peaks occur at 3 eV and 14 eV, respectively, which are related to π–electron plasmon peak. Also, for bulk MoS_2 in $E_{\|z}$ direction, the minimum of adsorption spectra is observed about 7 eV associated with the collective plasmons resonance, whereas the first and the highest peaks occur at 3.4 eV and 14.2 eV which are related to $(\pi + \sigma)$ electron plasmon peak. Besides, from this figure we can see that the transition in $E_{\|z}$ direction is more than that in $E_{\|x}$ direction. However, in comparison with the experiment result (the dashed line, which is adapted from the Ref. [44]) we see that the transition in $E_{\|x}$ direction is accordant with the experiment data more than the transition in $E_{\|z}$ direction is. This conclusion is also valid for optical reflectivity $R(\omega)$ in Fig. 4(c), where we showed the dependence of $R(\omega)$ on the energy.

Fig. 4(b) shows the adsorption spectra of monolayer MoS_2, there is shown that the minimum of the adsorption spectra is observed around 8.6 eV. The experimental data of the adsorption coefficient and reflectance of bulk MoS_2 is also plotted for

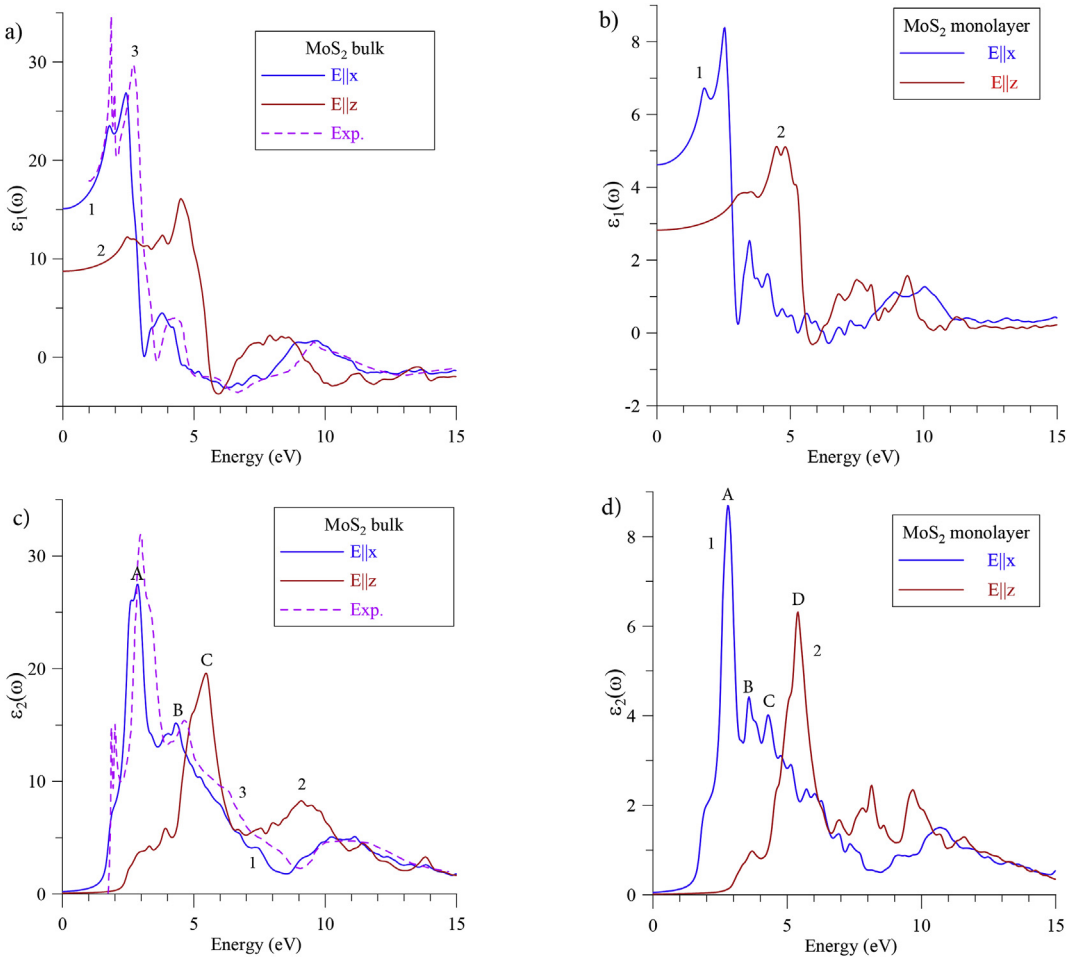

Fig. 3. Real $\varepsilon_1(\omega)$ and imaginary $\varepsilon_2(\omega)$ parts of dielectric function of bulk (a,c) and monolayer (b,d) MoS_2 calculated by GGA approximation in the cases of $E_{\|x}$ (1) and $E_{\|z}$ (2). The experimental data from Ref. [44] is shown by the dashed lines (3) for the case of bulk MoS_2 with the parallel electric field direction for comparison.

comparison. In comparison with the experimental data [44], we can see that our calculated adsorption spectra for both bulk and monolayer MoS_2 are associated with the energy of about 9 eV.

Fig. 5 shows the calculated refraction index $n^{ij}(\omega)$ and extinction index $k^{ij}(\omega)$ of bulk and monolayer MoS_2 under both directions of electric field. The refraction index and extinction index in both bulk and monolayer MoS_2 can be calculated by Ref. [45].

$$n^{ij}(\omega) = \frac{1}{\sqrt{2}}\left[\sqrt{\varepsilon_1^{ij}(\omega)^2 + \varepsilon_2^{ij}(\omega)^2} + \varepsilon_1^{ij}(\omega)\right]^{1/2}, \tag{5}$$

$$k^{ij}(\omega) = \frac{1}{\sqrt{2}}\left[\sqrt{\varepsilon_1^{ij}(\omega)^2 + \varepsilon_2^{ij}(\omega)^2} - \varepsilon_1^{ij}(\omega)\right]^{1/2}. \tag{6}$$

We can see that the static refraction index (the value of refraction coefficient at zero energy) in the $E_{\|x}$ direction of electric field of bulk and monolayer MoS_2 is 3.88 and 2.15, respectively and this value in the $E_{\|z}$ direction of electric field is 2.96 and 1.68, respectively.

The electron energy loss spectrum for bulk and monolayer MoS_2 in both parallel and perpendicular electric field direction is illustrated in Fig. 6. We all know that the electron energy loss function is a key factor which describes the energy loss of a fast electron traversing in the material. The sharp energy loss peak attributes to the plasma resonance and the corresponding frequency is the so-called plasma frequency. The energy loss function in terms of real and imaginary parts of dielectric constant can be defined as follows:

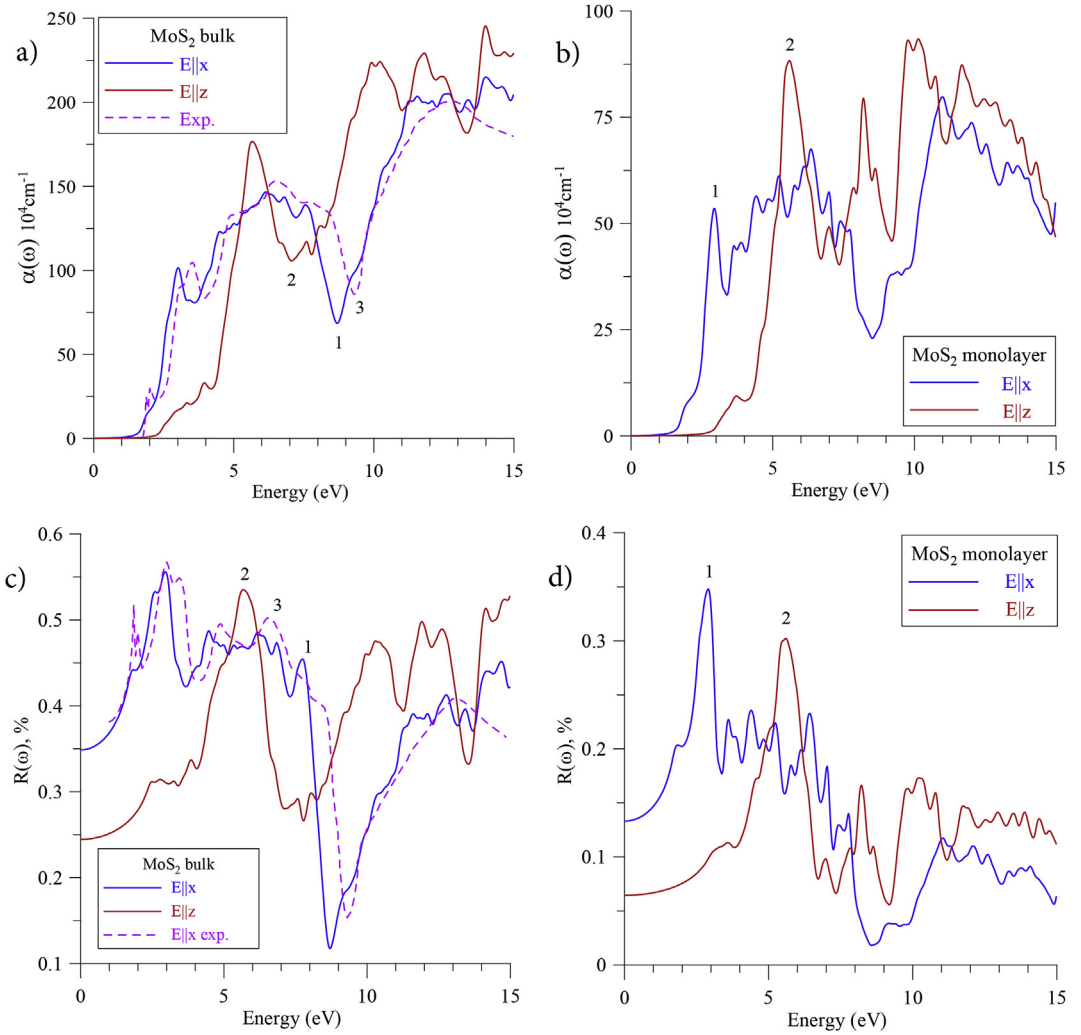

Fig. 4. Absorption coefficient $\alpha(\omega)$ (a, b) and optical reflectivity $R(\omega)$ (c, d) of bulk and monolayer MoS_2, respectively. (1) and (2) stand for the cases of $E_{\|x}$ and $E_{\|z}$, respectively. The dashed lines (3) in (a,c) are the experiment data from Ref. [44].

$$L^{ij}(\omega) = -\mathrm{Im}\left(\varepsilon^{-1}\right)^{ij} = \frac{\varepsilon_2^{ij}(\omega)}{\varepsilon_1^{ij}(\omega)^2 + \varepsilon_2^{ij}(\omega)^2}. \tag{7}$$

Fig. 6(a) shows the electron energy loss spectra for bulk MoS_2 in both perpendicular and parallel electric field directions. The experimental value is also plotted for comparison. As shown in Fig. 6(a), our calculated spectra shows the energy loss sharp peak of $E_{\|x}$ at 8.65 eV, which is consistent with the experimental value with energy loss peak at 8.81 eV [44]. In addition, we found a prominent peak at 23.1 eV in both parallel $E_{\|x}$ and perpendicular $E_{\|z}$ directions of electric field, as shown in the inset of Fig. 6(a). This value is consistent with experiment value of 23 eV in the energy loss spectra [44]. In Fig. 6(b) we show calculated electron energy loss spectra for both parallel $E_{\|x}$ and perpendicular $E_{\|z}$ direction of electric field in MoS_2 monolayer. It can be seen that for parallel $E_{\|x}$ electric field the sharp energy loss peak at 8.5 eV was observed in monolayer MoS_2. It is in agreement with the energy loss peak in bulk MoS_2 due to the collective plasmonic oscillations. It is clear that the traditional DFT method underestimates the band gap of materials like as semiconductors and insulators. Thus, it should be noted that the different calculated methods like as PBE, or hybrid functional may give rise to different values in determining the electronic structure, relative variations of the electronic properties, leading to the change in the optical properties of these materials.

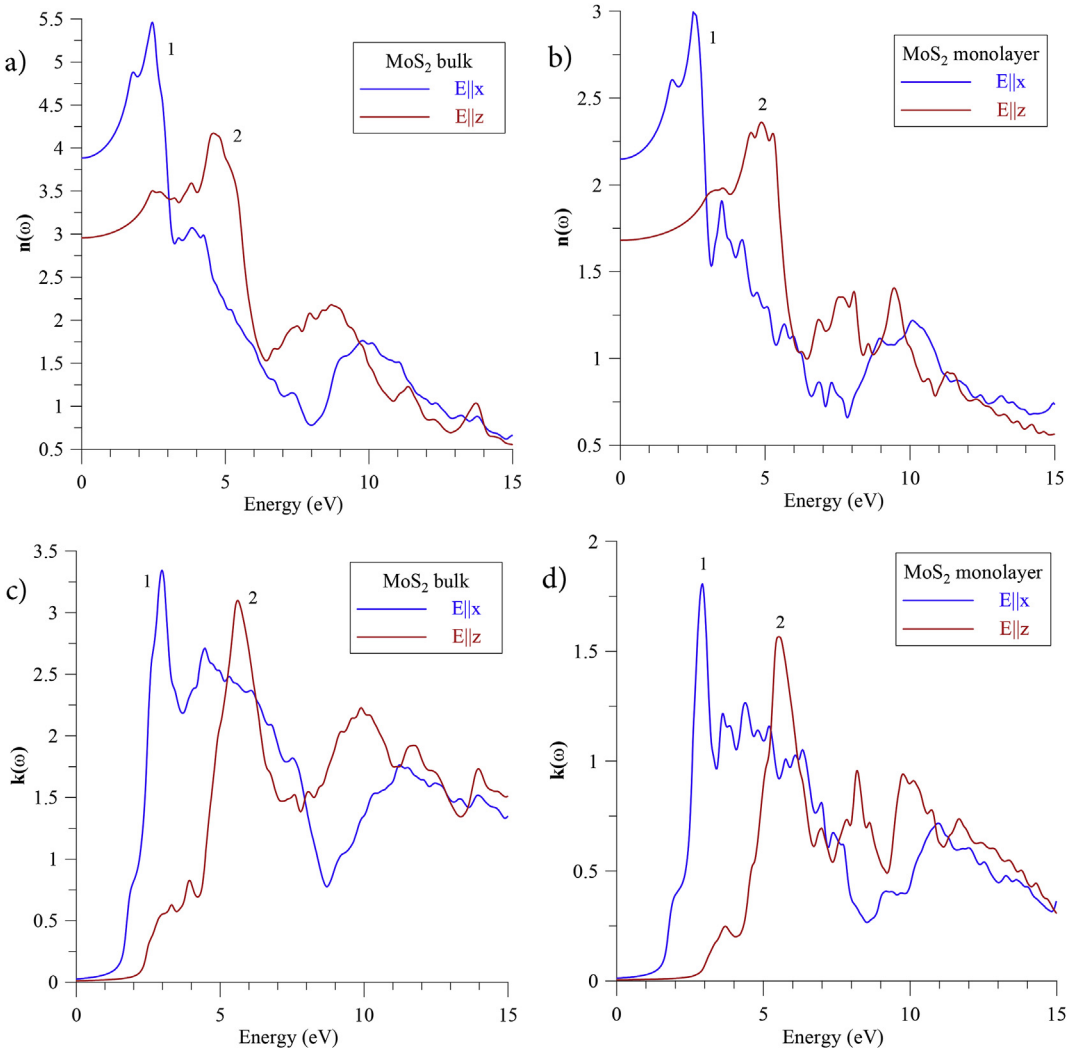

Fig. 5. Refractive index $n(\omega)$ and extinction coefficient $k(\omega)$ of MoS_2 bulk (a,c) and monolayer (b,d), respectively. (1) and (2) stand respectively for the cases of $E_{\|x}$ and $E_{\|z}$.

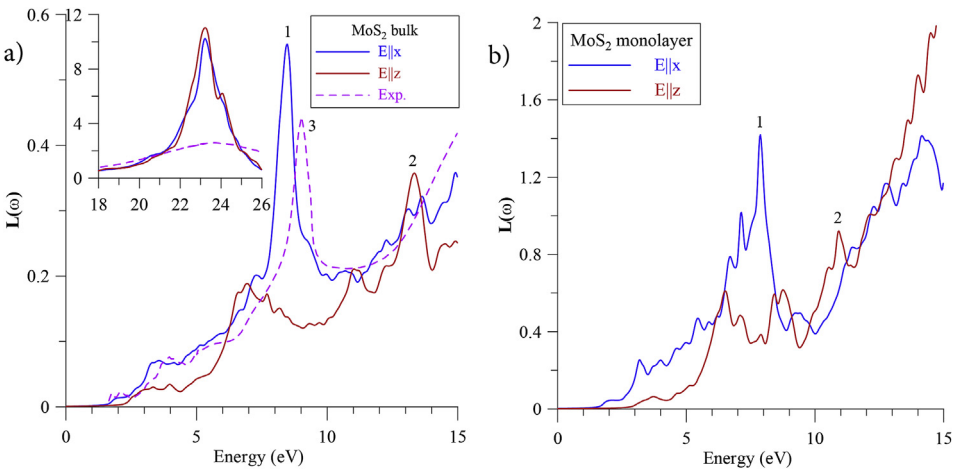

Fig. 6. Electron energy-loss spectrum $L(\omega)$ of bulk (a) and monolayer (b) MoS_2 in the cases of $E_{\|x}$ (1) and $E_{\|z}$ (2). The inset of (a) is the plot of $L(\omega)$ in the larger range of energy. The dashed line (3) in (a) is the experiment data from Ref. [44].

4. Conclusion

In conclusion, we study the optical properties of bulk and monolayer MoS_2 using DFT calculations. The obtained band gaps of 1.23 eV and 1.70 eV for the bulk and monolayer MoS_2, respectively, are in good agreement with the available data. For the optical characters of MoS_2, we investigated the dielectric function, optical reflectivity, and electron energy-loss spectrum in the energy range from 0 to 15 eV. Our DFT calculations showed that the difference in the dielectric constant between bulk and monolayer MoS_2 is significant in both directions of the electric field. The dielectric functions have highly anisotropic in the energy range from 0 to 6 eV but they become isotropic when the energy is larger than 7 eV. In comparison with bulk MoS_2, the appearance of the peak at 3.7 eV in the imaginary part of the dielectric function of monolayer MoS_2 demonstrates that quantum confinement can increase the interband transition in the monolayer MoS_2. The observed prominent peak at 23.1 eV in the energy-loss spectra agrees with experimental measurement. The obtained results may provide useful potential applications for the MoS_2 structures in electronic and optoelectronic devices.

Acknowledgments

This research is funded by Vietnam National Foundation for Science and Technology Development (NAFOSTED) under Grant Number 103.01-2016.07 and the Belarusian Scientific Program "Convergence".

References

[1] K.S. Novoselov, A.K. Geim, S.V. Morozov, D. Jiang, Y. Zhang, S.V. Dubonos, I.V. Grigorieva, A.A. Firsov, Electric field effect in atomically thin carbon films, Science 306 (2004) 666.
[2] F. Schwierz, Graphene transistors, Nat. Nanotechnol. 5 (2010) 487.
[3] D.G. Papageorgiou, I.A. Kinloch, R.J. Young, Mechanical properties of graphene and graphene-based nanocomposites, Prog. Mater. Sci. 90 (2017) 75.
[4] C. Neto, A.H.,F. Guinea, N.M.R. Peres, K.S. Novoselov, A.K. Geim, The electronic properties of graphene, Rev. Mod. Phys. 81 (1) (2009) 109.
[5] M. Sun, J.-P. Chou, Q. Ren, Y. Zhao, J. Yu, W. Tang, Tunable Schottky barrier in van der Waals heterostructures of graphene and g-GaN, Appl. Phys. Lett. 110 (17) (2017), 173105.
[6] M. Sun, W. Tang, Q. Ren, S. Wang, Jin Yu, Y. Du, Y. Zhang, First-principles study of the alkali earth metal atoms adsorption on graphene, Appl. Surf. Sci. 356 (2015) 668.
[7] K.F. Mak, C. Lee, J. Hone, J. Shan, T.F. Heinz, Atomically thin MoS_2: a new direct-gap semiconductor, Phys. Rev. Lett. 105 (13) (2010), 136805.
[8] Q. Tang, Z. Zhou, Z. Chen, Innovation and discovery of graphene-like materials via density-functional theory computations, in: Wiley Interdisciplinary Reviews: Computational Molecular Science vol. 5, 2015, p. 360.
[9] Q. Tang, Z. Zhou, Graphene-analogous low-dimensional materials, Prog. Mater. Sci. 58 (2013) 1244.
[10] M. Sun, W. Tang, Q. Ren, Y. Zhao, S. Wang, J. Yu, Y. Du, Y. Hao, Electronic and magnetic behaviors of graphene with 5d series transition metal atom substitutions: a first-principles study, in: Physica E: Low-dimensional Systems and Nanostructures vol. 80, 2016, p. 142.
[11] L.-J. Kong, G.-H. Liu, L. Qiang, Electronic and optical properties of O-doped monolayer MoS_2, Comput. Mater. Sci. 111 (2016) 416.
[12] M. Sun, J.-P. Chou, J. Yu, W. Tang, Electronic properties of blue phosphorene/graphene and blue phosphorene/graphene-like gallium nitride heterostructures, Phys. Chem. Chem. Phys. 19 (26) (2017), 17324.
[13] M. Sun, J.-P. Chou, Y. Zhao, J. Yu, W. Tang, Weak C-H…F-C hydrogen bonds make a big difference in graphane/fluorographane and fluorographene/fluorographane bilayers, Phys. Chem. Chem. Phys. 19 (41) (2017) 28127.
[14] M. Sun, Q. Ren, Y. Zhao, J.-P. Chou, J. Yu, W. Tang, Electronic and magnetic properties of 4d series transition metal substituted graphene: a first-principles study, Carbon 120 (2017) 265.
[15] D. Yang, S.J. Sandoval, W.M.R. Divigalpitiya, J.C. Irwin, R.F. Frindt, Structure of single-molecular-layer MoS_2, Phys. Rev. B 43 (14) (1991), 12053.
[16] M. Chhowalla, H.S. Shin, G. Eda, L.-J. Li, K.P. Loh, H. Zhang, The chemistry of two-dimensional layered transition metal dichalcogenide nanosheets, Nat. Chem. 5 (2013) 263.
[17] X. Huang, Z. Zeng, H. Zhang, Metal dichalcogenide nanosheets: preparation, properties and applications, Chem. Soc. Rev. 42 (5) (2013) 1934.
[18] Y. Cai, J. Lan, G. Zhang, Y.-W. Zhang, Lattice vibrational modes and phonon thermal conductivity of monolayer MoS_2, Phys. Rev. B 89 (3) (2014), 035438.
[19] Y. Cai, G. Zhang, Y.-W. Zhang, Polarity-reversed robust carrier mobility in monolayer MoS_2 nanoribbons, J. Am. Chem. Soc. 136 (17) (2014) 6269.
[20] Y. Jing, X. Tan, Z. Zhou, P. Shen, Tuning electronic and optical properties of MoS_2 monolayer via molecular charge transfer, J. Mater. Chem. 2 (2014), 16892.
[21] D. Kim, D. Sun, W. Lu, Z. Cheng, Y. Zhu, D. Le, T.S. Rahman, L. Bartels, Toward the growth of an aligned single-layer MoS_2 film, Langmuir 27 (18) (2011), 11650.
[22] K.S. Novoselov, D. Jiang, F. Schedin, T.J. Booth, V.V. Khotkevich, S.V. Morozov, A.K. Geim, Two-dimensional atomic crystals, Proc. Natl. Acad. Sci. U. S. A. 102 (2005), 10451.
[23] J.N. Coleman, M. Lotya, A. ONeill, S.D. Bergin, P.J. King, U. Khan, K. Young, A. Gaucher, S. De, R.J. Smith, I.V. Shvets, S.K. Arora, G. Stanton, H.-Y. Kim, K. Lee, G.T. Kim, G.S. Duesberg, T. Hallam, J.J. Boland, J.J. Wang, J.F. Donegan, J.C. Grunlan, G. Moriarty, A. Shmeliov, R.J. Nicholls, J.M. Perkins, E.M. Grieveson, K. Theuwissen, D.W. McComb, P.D. Nellist, V. Nicolosi, Two-dimensional nanosheets produced by liquid exfoliation of layered materials, Science 331 (2011) 568.
[24] Q.H. Wang, K. Kalantar-Zadeh, A. Kis, J.N. Coleman, M.S. Strano, Electronics and optoelectronics of two-dimensional transition metal dichalcogenides, Nat. Nanotechnol. 7 (2012) 699.
[25] C. Ataca, M. Topsakal, E. Aktürk, S. Ciraci, A comparative study of lattice dynamics of three- and two-dimensional MoS_2, J. Phys. Chem. C 115 (33) (2011), 16354.
[26] C.V. Nguyen, N.N. Hieu, Effect of biaxial strain and external electric field on electronic properties of MoS_2 monolayer: a first-principle study, Chem. Phys. 468 (2016) 9.
[27] C.V. Nguyen, N.N. Hieu, D.T. Nguyen, Dispersion-corrected density functional theory investigations of structural and electronic properties of bulk MoS_2: effect of uniaxial strain, Nanoscale Res. Lett. 10 (1) (2015) 433.
[28] P. Johari, V.B. Shenoy, Tuning the electronic properties of semiconducting transition metal dichalcogenides by applying mechanical strains, ACS Nano 6 (2012) 5449.
[29] J.-Y. Noh, H. Kim, Y.-S. Kim, Stability and electronic structures of native defects in single-layer MoS_2, Phys. Rev. B 89 (2014), 205417.
[30] A. Kumar, P. Ahluwalia, Tunable dielectric response of transition metals dichalcogenides MX_2 (M=Mo, W; X=S, Se, Te): effect of quantum confinement, Phys. B Condens. Matter 407 (24) (2012) 4627.
[31] A. Kumar, P. Ahluwalia, A first principle comparative study of electronic and optical properties of 1H-MoS_2 and 2H-MoS_2, Mater. Chem. Phys. 135 (2012) 755.

[32] W.B. Xu, B.J. Huang, P. Li, F. Li, C.W. Zhang, P.J. Wang, The electronic structure and optical properties of Mn and B, C, N co-doped MoS_2 monolayers, Nanoscale Res. Lett. 9 (2014) 554.
[33] A. Molina-Sánchez, K. Hummer, L. Wirtz, Vibrational and optical properties of MoS_2: from monolayer to bulk, Surf. Sci. Rep. 70 (4) (2015) 554.
[34] L.-p. Feng, J. Su, Z.-t. Liu, Effect of vacancies on structural, electronic and optical properties of monolayer MoS_2: a first-principles study, J. Alloy. Comp. 613 (2014) 122.
[35] C.V. Nguyen, N.N. Hieu, N.A. Poklonski, V.V. Ilyasov, L. Dinh, T.C. Phong, L.V. Tung, H.V. Phuc, Magneto-optical transport properties of monolayer MoS_2 on polar substrates, Phys. Rev. B 96 (12) (2017) 125411.
[36] P. Blaha, K. Schwarz, G.K.H. Madsen, D. Kvasnicka, J. Luitz, WIEN2k: an Augmented Plane Wave Plus Local Orbitals Program for Calculating Crystal Properties, Vienna University of Technology, Austria, 2001.
[37] J.P. Perdew, K. Burke, M. Ernzerhof, Generalized gradient approximation made simple, Phys. Rev. Lett. 77 (18) (1996) 3865.
[38] J.P. Perdew, K. Burke, M. Ernzerhof, Generalized gradient approximation made simple [Phys. Rev. Lett. 77, 3865 (1996)], Phys. Rev. Lett. 78 (7) (1997) 1396.
[39] P.E. Blöchl, O. Jepsen, O.K. Andersen, Improved tetrahedron method for brillouin-zone integrations, Phys. Rev. B 49 (23) (1994), 16223.
[40] J. Wilson, A. Yoffe, The transition metal dichalcogenides discussion and interpretation of the observed optical, electrical and structural properties,, Adv. Phys. 18 (1969) 193.
[41] H.S.S. Ramakrishna Matte, A. Gomathi, A.K. Manna, D.J. Late, R. Datta, S.K. Pati, C.N.R. Rao, MoS_2 and WS_2 analogues of graphene, Angew. Chem. Int. Ed. 49 (24) (2010) 4059.
[42] A. Delin, P. Ravindran, O. Eriksson, J. Wills, Full-potential optical calculations of lead chalcogenides, Int. J. Quant. Chem. 69 (3) (1998) 349.
[43] H. Tributsch, Solar energy-assisted electrochemical splitting of water. some energetical, kinetical and catalytical considerations verified on MoS_2 layer crystal surfaces, Zeitschrift für Naturforschung A 32 (9) (1977) 972.
[44] A. Beal, H. Hughes, Kramers-kronig analysis of the reflectivity spectra of 2H-MoS_2, 2H-$MoSe_2$ and 2H-$MoTe_2$, J. Phys. C Solid State Phys. 12 (5) (1979) 881.
[45] P. Ravindran, A. Delin, B. Johansson, O. Eriksson, J.M. Wills, Electronic structure, chemical bonding, and optical properties of ferroelectric and anti-ferroelectric $NaNO_2$, Phys. Rev. B 59 (3) (1999) 1776.